atmosphere

MDPI

Article

Elucidating Decade-Long Trends and Diurnal Patterns in Aerosol Acidity in Shanghai

Zhixiao Lv [1], Xingnan Ye [1,*], Weijie Huang [1], Yinghui Yao [1] and Yusen Duan [2]

[1] Shanghai Key Laboratory of Atmospheric Particle Pollution and Prevention (LAP3), National Observations and Research Station for Wetland Ecosystems of the Yangtze Estuary, Department of Environmental Science and Engineering, Fudan University, Shanghai 200438, China; 21210740069@m.fudan.edu.cn (Z.L.); 21110740007@m.fudan.edu.cn (W.H.); 19110740008@fudan.edu.cn (Y.Y.)

[2] Shanghai Environmental Monitoring Center, Shanghai 200235, China; duanys@sheemc.cn

* Correspondence: yexingnan@fudan.edu.cn

Abstract: Aerosol acidity is a critical factor affecting atmospheric chemistry. Here, we present a study on annual, monthly, and daily variations in $PM_{2.5}$ pH in Shanghai during 2010–2020. With the effective control of SO_2 emissions, the NO_2/SO_2 ratio increased from 1.26 in 2010 to 5.07 in 2020 and the NO_3^-/SO_4^{2-} ratio increased from 0.68 to 1.49. Aerosol pH decreased from 3.27 in 2010 to 2.93 in 2020, regardless of great achievement in reducing industrial SO_2 and NOx emissions. These findings suggest that aerosol acidity might not be significantly reduced in response to the control of SO_2 and NOx emissions. The monthly variation in pH values exhibited a V-shape trend, mainly attributable to aerosol compositions and temperature. Atmospheric NH_3 plays the decisive role in buffering particle acidity, whereas Ca^{2+} and K^+ are important acidity buffers, and the distinct pH decline during 2010–2016 was associated with the reduction of Ca^{2+} and K^+ while both temperature and SO_4^{2-} were important drivers in winter. Sensitivity tests show that pH increases with the increasing relative humidity in summer while it is not sensitive to relative humidity in winter due to proportional increases in H^+_{air} and aerosol liquid water content (ALWC). Our results suggest that reducing NOx emissions in Shanghai will not significantly affect $PM_{2.5}$ acidity in winter.

Keywords: $PM_{2.5}$; pH; diurnal variation; driving factor; Yangtze River Delta

Citation: Lv, Z.; Ye, X.; Huang, W.; Yao, Y.; Duan, Y. Elucidating Decade-Long Trends and Diurnal Patterns in Aerosol Acidity in Shanghai. *Atmosphere* **2024**, *15*, 1004. https://doi.org/10.3390/atmos15081004

Academic Editors: Milan Guzan and Tibor Vince

Received: 30 July 2024
Revised: 16 August 2024
Accepted: 19 August 2024
Published: 20 August 2024

1. Introduction

Aerosol acidity is a critically important indicator affecting human health and atmospheric chemistry. Aerosol acidity can affect chemical reactions; for example, the main oxidation pathway of SO_2 is related to the acidity of the aerosol [1,2]. With the increase in acidity, the solubility of transition metal ions (such as Fe^{2+} and Mn^{2+}) increases in atmosphere aerosol, the number of cations involved in the oxidation reaction increases, and then the ability to catalyze the oxidation of SO_2 is enhanced [3]. On the contrary, in neutral and alkaline atmospheres, the solubility of metal ions is low, the ability of metal ions to catalyze the oxidation of SO_2 decreases, and the oxidation of SO_2 by O_3 and NOx becomes the main way [4]. In addition, when the solubility of metal ions increases with the acidity of aerosols, the toxicity of aerosols is enhanced, which then affects the ecosystem [5–7]. Recently, significant correlations were confirmed between the pH value, water-soluble Fe, the concentration causing 20% inhibition of cell viability (IC20), and the concentration of exposure substance corresponding to a 1.5-fold increase in reactive oxygen species generation relative to control (EC1.5), indicating the strong impact of acidity on aerosol toxicity by increasing toxic equivalent concentrations of metals [8]. In addition, aerosol acidity can influence the acid-catalyzed heterogeneous reactions in the atmosphere, leading to a potential multiplication of secondary organic aerosol (SOA) mass [9,10]. Furthermore, aerosol acidity controls the phase distribution of semi-volatile compounds, such as HNO_3/NH_4NO_3 and $HCOOH/HCOONH_4$ systems [11,12].

Over the past decade, the Chinese government has implemented strict air pollution control strategies, such as the Air Pollution Prevention and Control Action Plan (2013–2017) and the three-year action plan for winning the blue-sky defense battle (2018–2020), leading to a significant reduction in $PM_{2.5}$ and great changes in aerosol chemical compositions. In the Yangtze River Delta (YRD), the proportion of sulfate in $PM_{2.5}$ was reduced from 18% to 14% between 2011 and 2018, while the proportion of nitrate increased from 24% to 29% [13,14]. Similarly, the concentration of $PM_{2.5}$ in Beijing significantly decreased from 88 μg m^{-3} in 2011 to 26 μg m^{-3} in 2020, and the mass ratio of NO_3^-/SO_4^{2-} in $PM_{2.5}$ increased from 0.88 to 1.70 during the same period [15].

The acidity of atmospheric particles has been extensively studied before. Based on model predictions that the aerosols were moderately acidic, Liu et al. (2017) questioned the role of the aqueous oxidization of SO_2 by NO_2 in sulfate productions in haze events in China [16]. For the highly acidic aerosols in Canada, aerosol pH has different responses to the changes in chemical composition in different seasons [17]. An observation in a northern city in China showed that aerosol pH values ranged between 0.33 and 13.6, and were highly dependent on the source contributions of water-soluble ions such as coal combustion, mineral dust, and vehicle exhaust [18]. Similarly, Sharma et al. (2022) highlighted the important role of SO_4^{2-}, NH_3, and K^+ in determining aerosol pH [19]. Fu et al. (2022) suggested that seasonal pH changes were mainly determined by aerosol compositions in Shanghai and reducing NH_3 emissions by 20% could not effectively mitigate winter $PM_{2.5}$ pollution but significantly increased particle acidity [20].

Changes in the aerosol chemical composition may change aerosol acidity. A model simulation showed that $PM_{2.5}$ pH increased from 4.4 to 5.4 during haze episodes in Beijing when the molar ratio of NO_3^-/SO_4^{2-} increased from 1 to 5 [21]. In contrast, another observation in Beijing showed that $PM_{2.5}$ pH in winter and autumn decreased significantly with elevated TNO_3 [22]. Model simulations showed that aerosol acidity strongly decreased over Europe and North America in recent decades while it increased over Asia [1]. This assumption was supported by observations in Guangzhou [23] and Beijing [24]. However, Zhou et al. (2022) reported that aerosol acidity increased in Shanghai in recent decades [25].

An in-depth analysis of aerosol pH changes is crucial for understanding long-term trends in aerosol pH and dominant drivers of pH variations, helping to predict pH in the future and formulate air pollution control strategies. This study investigated annual, monthly, and daily variations in $PM_{2.5}$ pH in Shanghai during 2010–2020. The main objectives of this study are (1) to elucidate the long-term trends in aerosol pH in highly urbanized areas over ten years; and (2) to explore the role of meteorological conditions and chemical compositions in driving pH changes.

2. Methods

2.1. Measurement Site and Instrumentation

The observation in this study was carried out in the downtown area of Shanghai during 2010–2021. The samples from 2010 to 2013 were collected on the roof of the No. 4 Teaching Building in the main campus of Fudan University (121.50° E, 31.30° N), and the samples from 2014 to 2021 were collected in the Pudong New Area Environmental Monitoring Station (121.54° E, 31.23° N), less than 10 km away from Fudan University (Figure S1). The two sites are surrounded by commercial and residential buildings, representing Shanghai's densely populated urban areas. There may be a small difference in aerosol composition between the two measurement sites.

A Monitor for Aerosols and Gases in Air (MARGA, ADI 2080, Metrohm Applikon B.V., Barendrecht, The Netherlands) with a time resolution of 1 h was used to determine aerosol SO_4^{2-}, NO_3^-, Cl^-, NH_4^+, Na^+, K^+, Ca^{2+}, and Mg^{2+}, and their gas precursors NH_3, HCl, and HNO_3. Due to the lack of MARGA data in 2012–2013, filter-based sampling with a time resolution of 24 h was used instead. Data were not available for 2011. Detailed information on MARGA was reported previously [20]. In brief, the water-soluble gases were absorbed by a wet rotating denuder while the water-soluble ions in the aerosols were

extracted using a steam jet aerosol collector. The collected gas and aerosol samples were analyzed online using a dual-channel ion chromatograph. Technical specifications for QA/QC followed local standards in the YRD region (DB31/T 310006-2021), which regulate that the correlation coefficients (r) for all targeted ions are larger than 0.995 [20]. The method detection limit of all components was 0.10 μg per cubic meter of air or better, except for K^+ (0.16 μg m^{-3}), Mg^{2+} (0.12 μg m^{-3}), and Ca^{2+} (0.21 μg m^{-3}) [26]. For filter-based sampling, QA/QC parameters for the determination of inorganic ions were previously reported [27]. Hourly meteorological data (temperature, relative humidity (RH), wind speed, and wind direction) were released by the China Meteorological Administration website. Hourly concentrations of $PM_{2.5}$, PM_{10}, SO_2, NO_2, CO, and O_3 were provided by Pudong Environmental Monitoring Center.

2.2. ISORROPIA II

ISORROPIA II is a computational and efficient aerosol thermodynamic equilibrium model, which has been widely used to calculate the thermodynamic equilibrium in the aerosol NH_4^+-SO_4^{2-}-NO_3^--Cl^--Na^+-Ca^{2+}-K^+-Mg^{2+}-H_2O system and the corresponding gas precursor [28]. ISORROPIA II operates in two modes: forward mode and reverse mode. In the forward mode, the input variables are temperature, RH, and the concentrations of TNH_3 (NH_3 and NH_4^+), TNO_3 (HNO_3 and NO_3^-), TCl (HCl and Cl^-), SO_4^{2-}, Na^+, Ca^{2+}, K^+, and Mg^{2+}. In the reverse mode, the input variables are ambient temperature, RH, and the concentrations of SO_4^{2-}, NO_3^-, Cl^-, NH_4^+, Na^+, Ca^{2+}, K^+, and Mg^{2+}. The output of both modes is aerosol liquid water content (ALWC), hydrogen ion content, and the concentration of species in the gas and aerosol phases [29]. The forward model predicts aerosol composition and gas-particle partitioning much more accurately than the reverse model, because the forward model uses gas and aerosol inputs, effectively limiting the impact of measurement errors [30]. Therefore, our study chose to run the forward mode and assumed that the aerosol was metastable with no solid precipitation. Aerosol pH is defined as follows:

$$pH = -log_{10}\gamma_{H^+}H^+_{aq} = -log_{10}\left(\frac{\gamma_{H^+}H^+_{air}}{ALWC}\right) \quad (1)$$

where γ_{H^+} refers to the activity coefficient of hydrogen ion (assumed to be 1). H^+_{aq} (mol L^{-1}) and H^+_{air} (ng m^{-3}) are the concentrations of H^+ in aqueous particles and ambient air, respectively. ALWC (μg m^{-3}) is the water uptake by inorganic species.

Overall, nitrate in the particle phase was underestimated when RH was lower than 40% since urban particles possibly dehydrate at RH below 40% [20]. When RH is above 95%, ALWC may grow exponentially with RH, resulting in large uncertainties of pH [31]. Therefore, samples collected at RH > 95% and RH < 40% were discarded in the study.

3. Results and Discussion

3.1. Long-Term Variations in the Nitrate-to-Sulfate Ratio

Figure 1 shows the decade changes in SNA (sulfate, nitrate, and ammonium) and corresponding gas precursors from 2010 to 2020. The annual variation in atmospheric SO_2 showed a distinct downward trend, from an average of 28.8 ± 10.8 μg m^{-3} in 2010 to 7.1 ± 2.8 μg m^{-3} in 2020. In contrast, the long-term trend in atmospheric NO_2 was relatively flat, with an average of 38.7 μg m^{-3} in 2010 and 36.1 μg m^{-3} in 2020. As a result, the atmospheric ratio of NO_2/SO_2 increased from 1.26 in 2010 to 5.07 in 2020. Like their gas precursors, the sum concentration of sulfate plus nitrate decreased from approximately 20 μg m^{-3} to less than 12 μg m^{-3}, a decline of 40%. The lower SNA concentration in 2010 relative to the following years might be attributed to different sampling locations. The mass ratio of nitrate to sulfate (NO_3^-/SO_4^{2-}) increased from 0.68 to 1.49, with a ratio below 1.0 before 2015. Ye et al. (2021) reported that NO_3^-/SO_4^{2-} in rainwater increased from approximately 0.3 to above 1.0 during the same period [32], consistent

with the aerosol NO_3^-/SO_4^{2-} ratio. The lower ratio of NO_3^-/SO_4^{2-} in rainwater might be associated with the in-cloud reactions of SO_2. It is worth noting that the ratio of NO_3^-/SO_4^{2-} was always less than that of NO_2/SO_2 due to the longer atmospheric life of SO_2. These variations can be attributable to the non-proportional reduction of SO_2 and NO_x emissions. As illustrated in Figure S2, industrial SO_2 emissions in Shanghai were reduced from 2.2×10^5 tons in 2010 to 5.2×10^3 tons in 2020, indicating that the industrial desulfurization and clean energy substitution strategies have achieved great success. Since the reduction in industrial NOx emissions was almost offset by the increasing number of on-road vehicles, NOx pollution shifted from industry-dominated to vehicle-dominated in 2016. Generally, the total emissions of acidic pollutants were significantly reduced. Meanwhile, the concentration of Ca^{2+} dropped by 76% during the observation period, indicating the significant achievement in the control of soil dust and the weakened capacity to neutralize atmospheric acidity. These findings suggest that aerosol acidity might not be significantly reduced in response to the control of SO_2 and NO_x emissions.

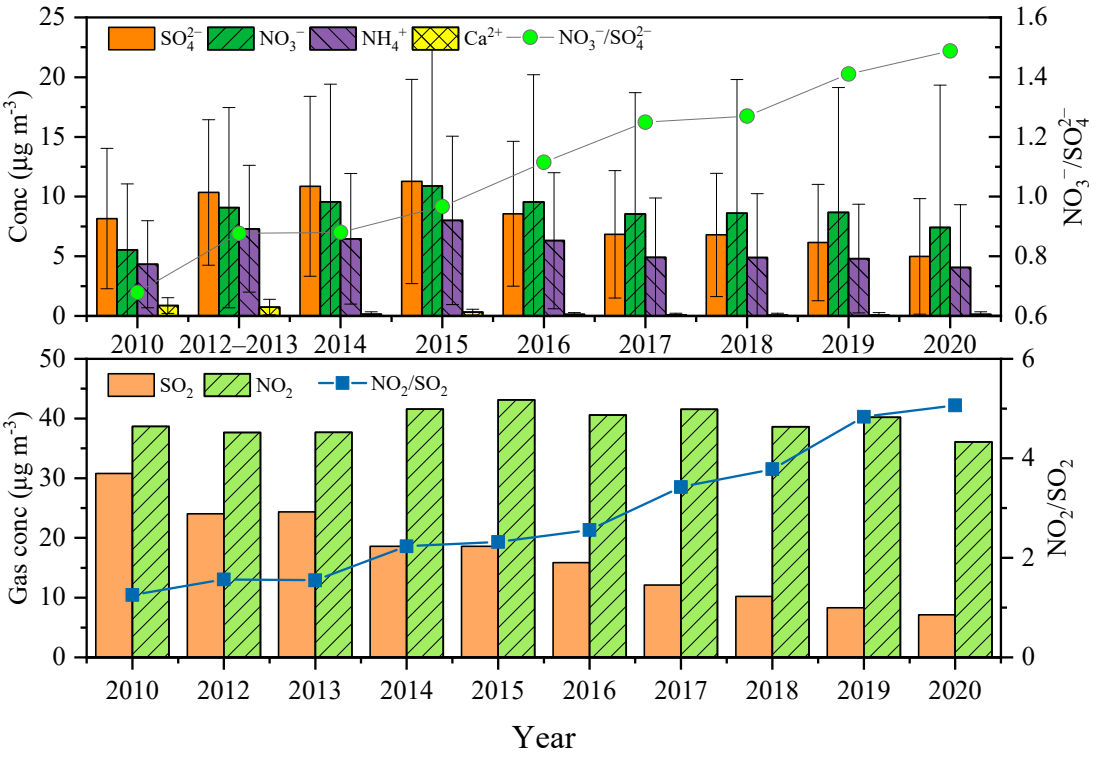

Figure 1. Annual average concentrations of major ions and acidic gas pollutants during 2010–2020.

3.2. Variation Trend in Aerosol pH

3.2.1. Annual Variations in Aerosol pH

Figure 2 shows the long-term trend in aerosol pH in Shanghai over the decade from 2010 to 2020. The aerosol acidity showed an overall enhanced trend, with the annual average pH decreasing from 3.27 in 2010 to 2.93 in 2020. We should point out that the potential contributions of secondary organic aerosols to water uptake and organic acids to H^+ are not considered in this study, contributing to uncertainty in aerosol pH assessment. In contrast to the atmospheric sulfate and nitrate decrease by 40% over the decade, aerosol acidity increased by 0.34 units pH, supporting the idea that aerosol acidity responded nonlinearly to SO_2 and NO_x emission control. Similar to our results, an annual pH decline rate of around 0.04 units was reported previously [25]. The small discrepancies between the two studies could be attributed to different sampling locations and statistical methods. The pH of rainwater increased by 0.8 units during the same period [32], possibly because rain droplets can scavenge alkaline coarse particles. The median pH for each year was generally

higher than the mean, indicating that the distribution of hourly pH was skewed to the lower pH direction. The changing trend in aerosol pH displays a two-stage shape, with a distinct decrease during 2010–2016 and a weaker variation from 2016 to 2020. Meanwhile, the concentration of Ca^{2+} decreased from 0.85 μg m^{-3} to 0.13 μg m^{-3} from 2010 to 2016 while it remained around 0.1 μg m^{-3} from 2016 to 2020, indicating that the nonvolatile cations were important drivers affecting the decade aerosol pH variations.

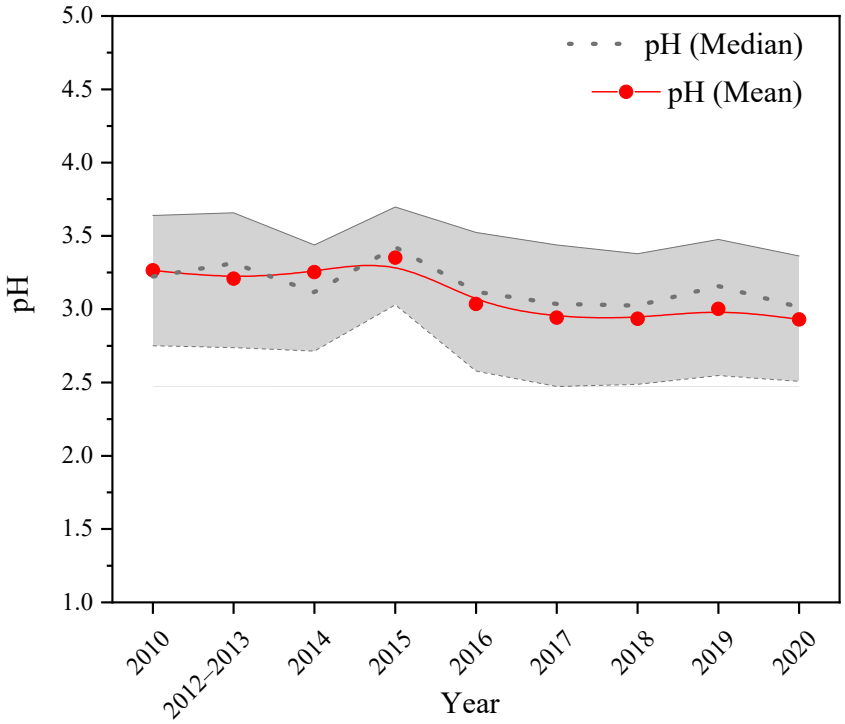

Figure 2. Annual variation in aerosol pH during 2010–2020 in Shanghai. The shaded area shows the range of 25% to 75% of the hourly observational data.

Table 1 summarizes aerosol pH in different measurement sites over the world. The overall aerosol pH in Shanghai (3.1 ± 0.6) was comparable to Nanjing (3.3 ± 0.1) and Wuhan (3.0 ± 1.0) in the middle and lower reaches of the Yangtze River, but significantly lower than that of Beijing (4.2 ± 0.4) and Tianjin (4.9 ± 1.4) in North China. Intriguingly, these aerosols with high loadings of sulfate and nitrate were weakly acidic while the aerosols were highly acidic (pH ≈ 1.0) in less-polluted Alabama and Crete where sulfate and nitrate loadings were much lower, indicating that aerosol acidity was not necessarily consistent with the mass loadings of sulfate and nitrate. As shown in Table 1, aerosol pH was positively correlated with the concentration of atmospheric NH_3, suggesting that ammonia was the major driving factor affecting global particle acidity distributions. Wang et al. (2016) attributed the difference between highly acidic London smog in 1952 and less acidic Beijing aerosols in 2012 to NH_3 levels [33]. The lower pH in Guangzhou than in Shanghai might be attributed to higher temperatures. These findings indicated that aerosol pH was much more sensitive to the amount of atmospheric NH_3 available for neutralizing acidic sulfate and nitrate. In addition, nonvolatile cations such as Na^+, K^+, Ca^{2+}, and Mg^{2+} could affect aerosol acidity when their concentrations were significant relative to anions [34]. To validate the central role of NH_3, aerosol pH in Pasadena and Beijing was re-calculated by inputting the average NH_3 concentration in Shanghai (5.4 μg m^{-3}). The re-calculated pH increased from 2.7 to 4.0 in Pasadena as the NH_3 concentration increased from 0.8 to 5.4 μg m^{-3} and decreased from 4.2 to 3.5 in Beijing as the NH_3 concentration decreased from 18.3 to 5.4 μg m^{-3}, confirming that both ammonia and alkaline nonvolatile cations were important buffers of aerosol acidity.

Table 1. Concentrations of major inorganic ions and aerosol pH in different measurement sites worldwide (unit: μg m^{-3}).

No.	Location	SO_4^{2-}	NO_3^-	NH_4^+	NH_3	pH	Reference
1	Shanghai, CN	8.3 ± 6.6	8.5 ± 10.8	5.6 ± 5.7	5.4 ± 3.7	3.1 ± 0.6	This study
2	Nanjing, CN	23.2 ± 0.7	16.9 ± 1.7	5.3 ± 0.6	/	3.3 ± 0.1	[35]
3	Wuhan, CN	10.1 ± 6.1	10.2 ± 9.2	8.0 ± 5.9	9.9 ± 5.4	3.0 ± 1.0	[36]
4	Guangzhou, CN	9.9 ± 5.9	4.0 ± 4.3	3.8 ± 3.0	8.7 ± 5.8	2.5 ± 0.7	[37]
5	Beijing, CN	7.7 ± 7.5	13.6 ± 16.1	7.4 ± 7.8	18.3 ± 7.8	4.2 ± 0.4	[22]
6	Tianjin, CN	8.9 ± 1.3	10.7 ± 2.8	6.9 ± 1.8	/	4.9 ± 1.4	[18]
7	Alabama, US	1.7 ± 1.2	0.1 ± 0.1	0.5 ± 0.3	0.4 ± 0.3	1.0 ± 0.5	[38]
8	Pasadena, US	1.9 ± 0.7	3.7 ± 1.5	1.8 ± 0.7	0.8 ± 0.6	2.7 ± 0.3	[11]
9	Crete, GR	2.3 ± 1.6	0.1 ± 0.1	0.8 ± 0.6	/	1.3 ± 1.1	[39]
10	Harrow, CA	7.2 ± 1.1	0.5 ± 0.4	2.0 ± 0.2	1.7 ± 0.2	2.5 ± 1.5	[40]
11	Indo-Gangetic Plain, India	18.6 ± 5.8	1.1 ± 0.8	20.3 ± 5.2	/	3.0 ± 0.2	[19]
12	Cabauw, NL	2.2 ± 0.3	4.3 ± 1.2	1.8 ± 0.3	7.4 ± 2.8	3.6 ± 0.3	[41]
13	Po Valley, Italy	1.8 ± 1.1	8.2 ± 5.9	3.3 ± 2.0	/	3.7 ± 0.6	[42]

CN: China; US: United States; CA: Canada; GR: Greece; NL: Netherlands.

3.2.2. Seasonal Variations in Aerosol pH

Figure 3 illustrates the long-trend in seasonal pH values from 2010 to 2020. The monthly variation in pH values exhibited a V-shape trend, decreasing from February and increasing from September. Aerosol pH in August was the lowest (with an average of less than 2.5) and the fluctuation range was the largest. From a seasonal perspective, aerosol pH followed the order of winter > spring > autumn > summer, indicating that ambient temperature was an important driver for pH variation. In this study, the seasons from spring to winter are defined as the period from March to May, June to August, September to November, and December to February, respectively. Similar seasonal pH trends were reported previously [17,22,36,38,43]. As indicated by Equation (1), aerosol pH depends on H^+_{air} and ALWC, which are functions of pollutant concentrations, temperature, and RH. Elevated ALWC by increasing RH can dilute H^+_{aq} and increase pH as well as promoting nitrate formation via nighttime N_2O_5 hydrolysis. The approximately one-unit difference in pH between winter and summer was mainly attributed to aerosol compositions because a doubling ALWC in winter increases aerosol pH by only 0.3 units [20]. Although temperature is not a parameter in Equation (1), it greatly affects the photooxidation rate of SO_2 and NOx and the gas-particle partitioning of semi-volatile NH_4NO_3 and NH_4Cl, with an indirect effect on aerosol acidity. During 2010–2015, the seasonal average pH showed a steady downward trend in winter while remaining stable in summer and autumn, resulting in a decline in the seasonal pH difference from 1.14 to 0.72. Interestingly, the seasonal difference in pH returned to approximately 1.0 in 2016–2020. In addition, the seasonal average pH was unexpectedly high in the summer and autumn of 2015. The mechanisms driving seasonal pH variations will be discussed in the next sections.

3.2.3. Diurnal Variation in Aerosol pH

Figure 4 illustrates the diurnal variation in aerosol pH along with ALWC and the mass ratio of NO_3^-/SO_4^{2-}. Overall, aerosol pH began to decrease in the early morning, reaching the minimum values at noon, followed by a continuous increase in the afternoon and high values at night, further supporting the temperature dependence on aerosol acidity. In summer, the average pH values at night were approximately 0.4–0.7 units larger than those at noon. With the strongest acidity, the aerosol noon minimum dropped to nearly 2.1 in 2016. Similar to summer, aerosol pH in winter showed a V-shaped diurnal trend but the diurnal range was much narrower. In 2020, the daily variation in aerosol pH narrowed to below 0.3 units. Contrary to our results, the diurnal variation in aerosol pH over the southeastern United States was approximately one unit larger in winter than in summer [38], indicating that the diurnal pH trends are highly related to the regional pollution background.

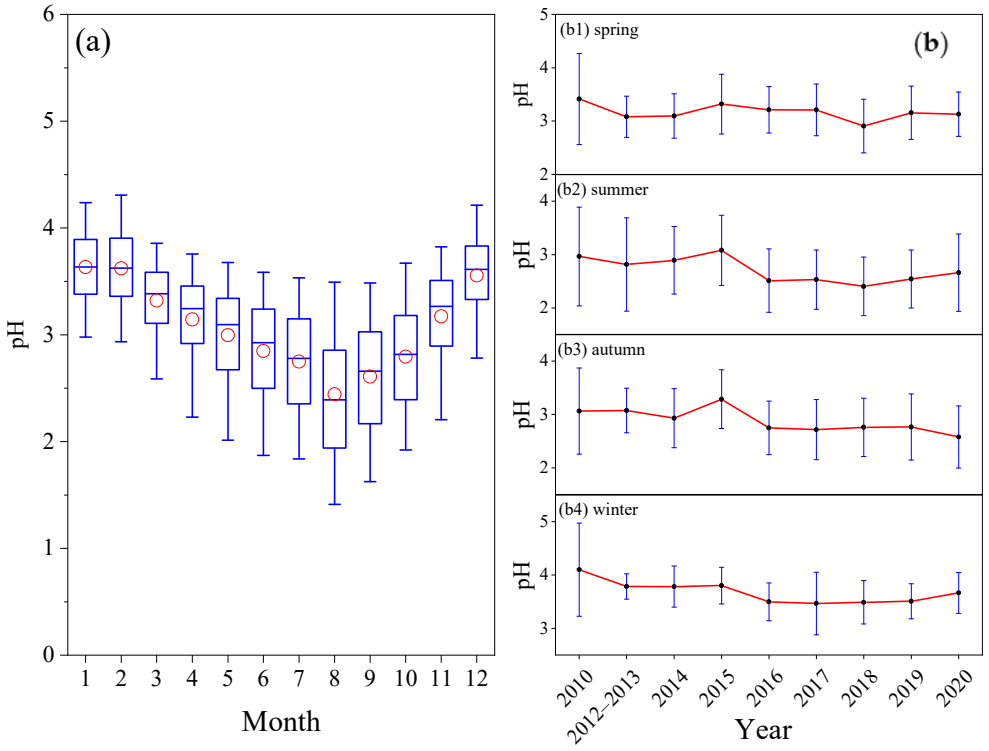

Figure 3. Seasonal variation in aerosol pH during 2010–2020 in Shanghai. (**a**) The box spans the range from the 25th to the 75th percentiles and the whiskers denote the 5th and 95th percentiles. The red circle in the box represents the average. (**b**) The error bar represents one standard deviation.

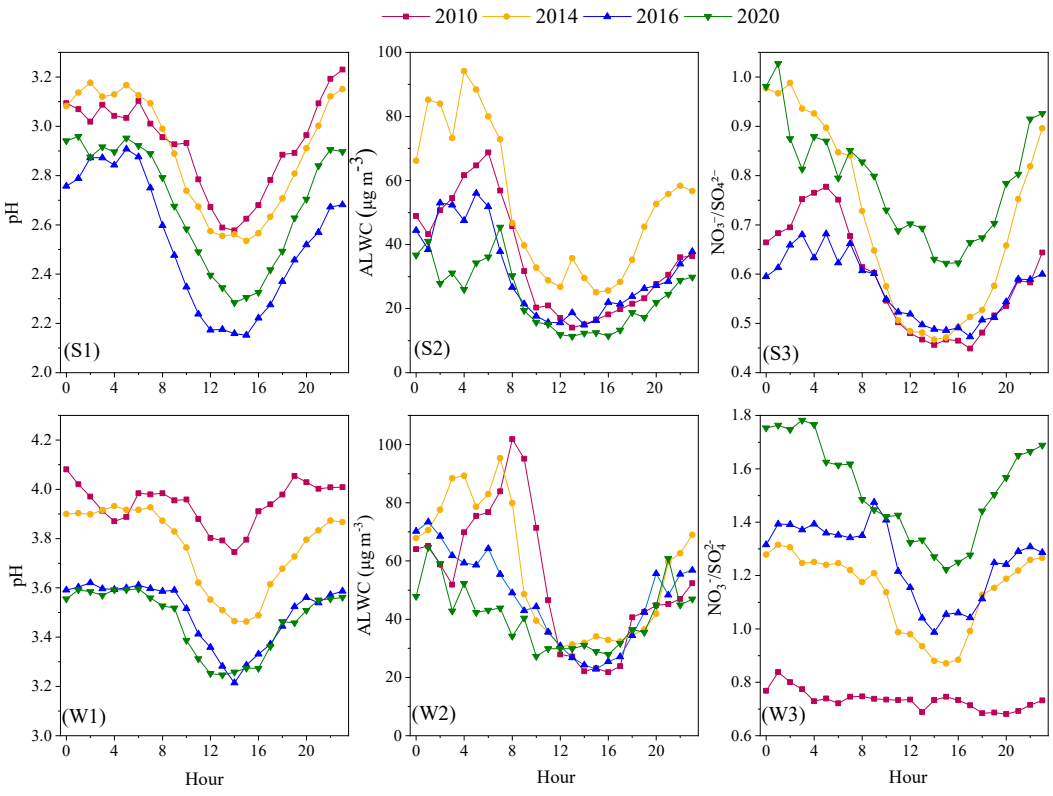

Figure 4. Diurnal variation in aerosol pH along with ALWC and NO_3^-/SO_4^{2-} in 2010–2020. (**S1**): pH in summer; (**S2**): ALWC in summer; (**S3**): NO_3^-/SO_4^{2-} in summer; (**W1**): pH in winter; (**W2**): ALWC in winter; (**W3**): NO_3^-/SO_4^{2-} in winter.

Both ALWC and NO_3^-/SO_4^{2-} followed a similar diurnal pattern as pH, indicating that they provided an additive effect on pH variation. As ALWC is a function of RH and the total amount of hygroscopic aerosols, ALWC generally peaked in the early morning and rapidly decreased after sunrise. ALWC at noon was reduced by 50–70% relative to the early morning, corresponding to a pH increase of 0.3–0.5 units, indicating that ALWC was the main driver for the strong diurnal pH variation. The flat diurnal pattern of the NO_3^-/SO_4^{2-} ratio in 2010 indicates an insignificant effect of chemical composition on the diurnal trend in pH, providing a reasonable explanation for the narrowest diurnal variation in pH.

From the perspective of aerosol composition, sulfate and nitrate are regarded as the major driving factors of diurnal patterns in pH [38]. When sulfate and nitrate are neutralized primarily by ammonium, the concentration of H^+ is controlled primarily by the thermodynamic equilibrium between particle-phase NH_4^+ and gaseous NH_3. As $(NH_4)_2SO_4$ is less volatile than NH_4NO_3, the elevated sulfate leads to a much greater increase in H^+_{air} than that of TNO_3. NH_4NO_3 tended to evaporate with increasing temperature and decreasing ALWC during the daytime. In contrast, uptake on humid particles was favored at night due to its dissociation being highly sensitive to temperature and RH changes, resulting in a V-shaped diurnal pattern. The NO_3^-/SO_4^{2-} ratio in winter was significantly larger than in summer, which can be partly responsible for the weaker acidity of winter aerosols.

3.3. Quantitative Analysis of pH Drivers

3.3.1. Effect of Alkaline Buffers on Interannual pH Variations

As aforementioned, ammonia is the major alkaline buffer for aerosol pH globally while nonvolatile cations exhibit a non-negligible impact on aerosol pH when their concentrations become significant. In this study, temperature, relative humidity, and concentrations of chemical composition were averaged for each summer and winter (Table S1). Figure 5 illustrates the aerosol pH predicted by the average concentrations and the buffer effect of NH_3 and nonvolatile cations on summer and winter aerosols. The aerosol pH values predicted by the averaged concentrations of chemical composition and meteorological parameters are close to those averaged by hourly pH values, indicating that they can represent the typical pH trends. The inserted images represent the predicted aerosol pH values by setting the concentration of NH_3 to zero while the other variables are fixed at their average values. It is worth noting that aerosol pH would be below zero in the absence of NH_3, emphasizing the decisive role of NH_3 in buffering particle acidity. Similar to NH_3, aerosol pH is predicted by inputting the concentrations of Ca^{2+} and K^+ as 0 while other variables are fixed (Table S2). The buffering effects of Ca^{2+} and K^+, ΔpH, are obtained by comparing the pH decline when the concentrations of Ca^{2+} and K^+ are set to 0. Ca^{2+} and K^+ are tracers of crustal dust and biomass burning, respectively. Coal combustion is another important source of K^+ in many Chinese cities [20]. The buffing effect of Ca^{2+} was more significant than K^+ before 2013, but K^+ remained higher in 2014–2015. The combined buffing effect of Ca^{2+} and K^+ decreased by 0.4 units of pH during the winter of 2010–2016, corresponding to the aerosol pH decline during this period, indicating that the reduction in acidic pollutant emissions was largely offset by the reduction in alkaline buffers. During 2016–2020, the buffing effect of nonvolatile cations could be ignored in summer while the buffing effect of K^+ remained at approximately 0.4 units pH in winter. Long-range pollutant transport from north China contributes greatly to the increase in K^+ concentration and $PM_{2.5}$ pollution in Shanghai because the prevailing wind direction in Shanghai varies from northwest to northeast in the winter [26,44]. The increase in K^+ in winter was possibly related to the transportation of biomass burning and coal combustion pollutants under the regime of prevailing winds from the north. In contrast to aerosol pH below zero in the absence of NH_3, the largest buffering effect of nonvolatile cations was less than 0.6 units pH, emphasizing the decisive role of NH_3 in buffering particle acidity.

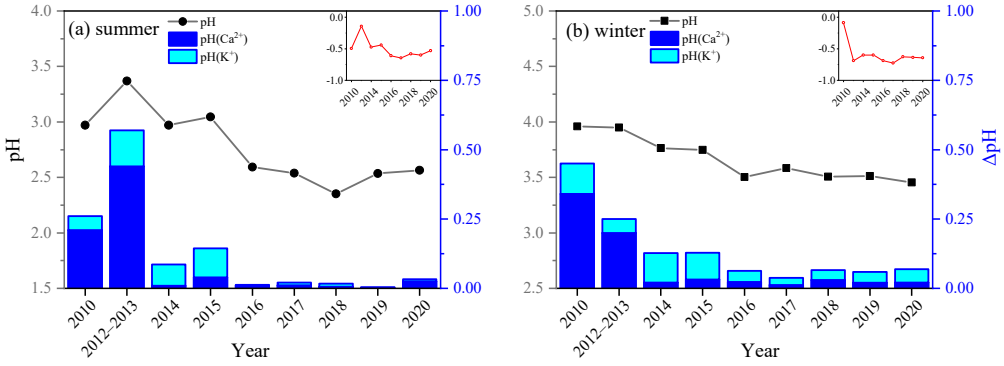

Figure 5. Contribution of alkaline buffers to aerosol acidity. The black line represents the predicted aerosol pH based on the annual average parameters. The column chart illustrates the buffer effect from Ca^{2+} and K^{+}. The inserted image represents the predicted pH by setting the concentration of NH_3 to zero.

3.3.2. Effects of Meteorological Parameters and Chemical Composition on Diurnal pH Variations

The contributions of individual driving factors to diurnal pH variations are estimated in Figure 6 and Tables S4–S7. Similar to the above section, the effect of a driving factor on aerosol pH is evaluated by replacing this factor at 10:00, 14:00, 20:00, and 24:00 with the value at 5:00 in the morning. The reference point is set at 5:00 when aerosol pH was generally the highest. In both summer and winter, the temperature during the day was higher than that at night, while the humidity was just the opposite. The increase in temperature can reduce aerosol pH by partitioning aerosol NH_4NO_3 and NH_4Cl into the gas phase, leading to decreases in NO_3^-/SO_4^{2-} and pH [41]. The effect of RH on aerosol pH is more complicated. On the one hand, elevated RH can enhance ALWC which dilutes the ionic concentration. On the other hand, the increase in ALWC favors more gaseous NH_3 and HNO_3 partitioning into the particle phase. The diurnal pH variation in summer was mainly driven by temperature and RH. Only a 7 °C increase in temperature is required for a 0.5 unit drop in pH, which is lower than that in Canada [17], possibly due to the higher mass loading of secondary inorganic aerosols in our study. As shown in Tables S4 and S6, the narrow fluctuations of dew point temperature (T_d) indicate that the diurnal RH variations were mainly driven by temperature, further highlighting the important role of temperature in the diurnal variations in aerosol pH. The effects of SO_4^{2-}, TNO_3, and TNH_3 were much weaker than those of temperature and RH in summer. It is worth noting that both elevated SO_4^{2-} and decreased NO_3^- in the daytime contributed to the decreasing aerosol pH. In contrast, the main drivers of diurnal pH variation in winter were temperature and SO_4^{2-}. Another significant difference from summer was that the decreasing RH could enhance aerosol pH in winter. It is worth noting that RH played a minor role in diurnal pH patterns in winter. In summary, the diurnal variation in aerosol pH in summer is mainly affected by temperature and RH, while the diurnal variation in aerosol pH in winter is sensitive to both meteorological parameters and aerosol chemical composition.

For an in-depth understanding of the effect of meteorological parameters and chemical composition on aerosol pH, sensitivity tests were performed based on two cases of summer and winter aerosols (Figure 7). The concentration of NH_4^+ decreased nonlinearly with the increase in temperature because the concentration product of NH_3 and HNO_3 is an exponential function of temperature [4]. Aerosol pH almost linearly decreased with the increase in temperature since the concentration of H^+ in ambient air $\left(H_{air}^+\right)$ almost exponentially increases with the increasing temperature. Although ALWC always increased with the increase in RH, H_{air}^+ displayed different trends between summer and winter. In summer, H_{air}^+ first decreased with the increase in RH which favors more gaseous NH_3 partitioning into the aerosol water. In contrast, H_{air}^+ in winter increased with the increase in RH, leading to a slight pH decrease at RH < 80%. As shown in Figure 7e,f, the concentration of NH_4^+ increased linearly with the increase of SO_4^{2-} due to the higher affinity of H_2SO_4

to NH_3. However, the hygroscopic growth of $(NH_4)_2SO_4$ was lower than that of NH_4NO_3, indicating that aerosol pH decreased with the decrease of NO_3^-/SO_4^{2-}. In contrast, the concentration of aerosol NH_4^+ only slightly increased with the increasing TNO_3 in summer due to most of the TNO_3 partition to the gas phase. Aerosol pH increased with the increase in TNO_3 due to the increase in NO_3^-/SO_4^{2-}. In winter, aerosol pH increased slightly with the increase in TNO_3 for $NO_3^-/SO_4^{2-} < 1.5$. However, aerosol pH slightly decreased with the increase in TNO_3 for higher NO_3^-/SO_4^{2-}. An observation in Beijing showed that $PM_{2.5}$ pH increased with increasing NO_3^-/SO_4^{2-} [21], while another observation found that $PM_{2.5}$ pH decreased with increasing TNO_3 [22]. This finding suggests that the impact of NO_3^-/SO_4^{2-} on pH depends on the pollution background, providing a reasonable explanation for the different trends observed in Beijing. Our results suggest that reducing NOx emissions in Shanghai will not significantly affect $PM_{2.5}$ acidity in winter.

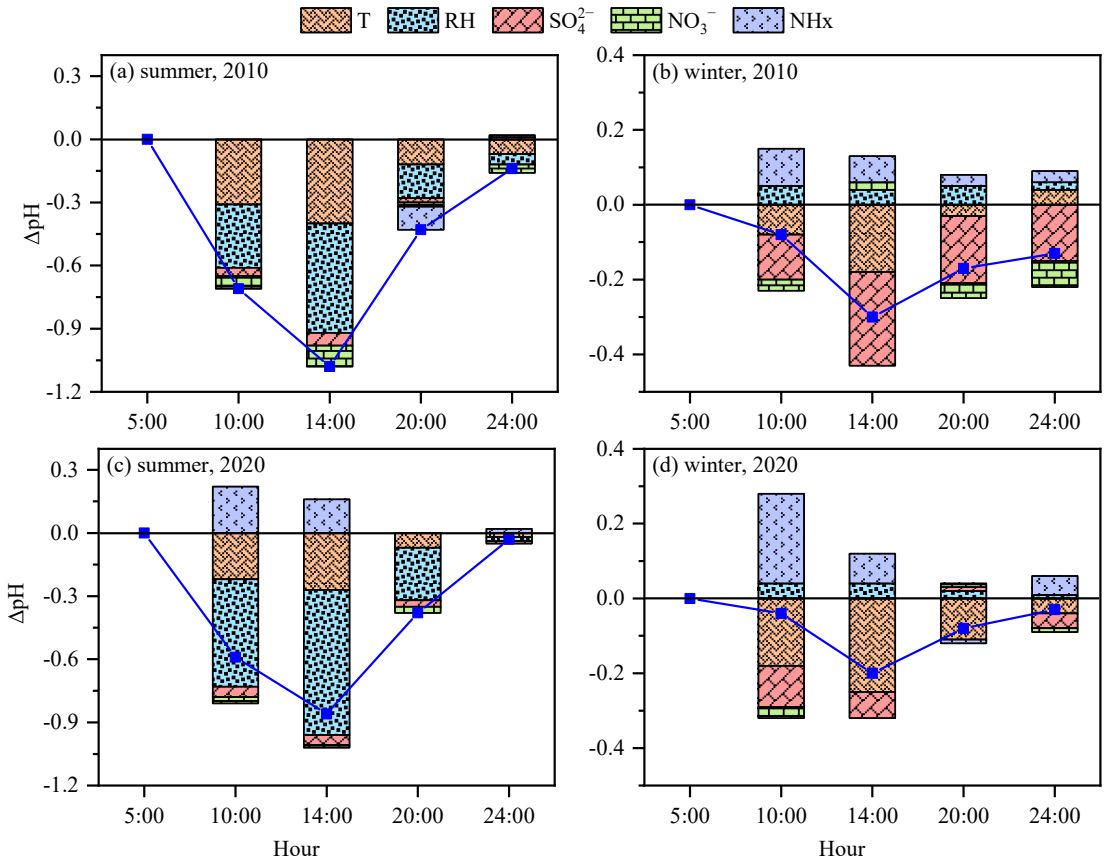

Figure 6. Contributions of chemical composition and meteorological parameters to the diurnal pH variation. The blue scatter line represents the diurnal pH variation with pH at 5:00 am as the baseline. The stacked column chart represents the contribution of each driving factor to ΔpH.

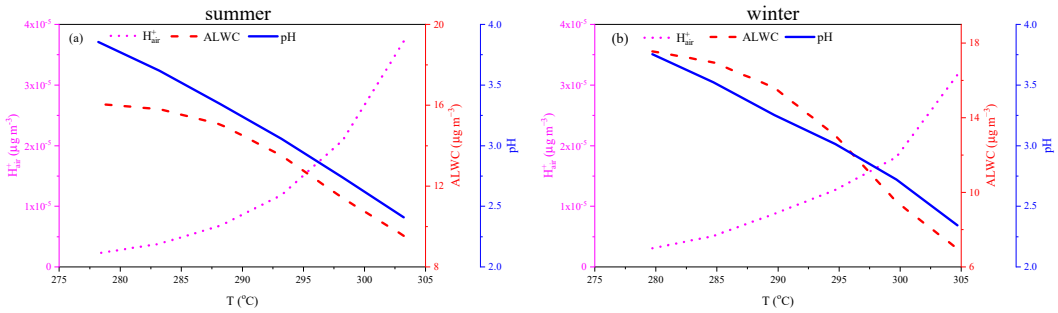

Figure 7. *Cont.*

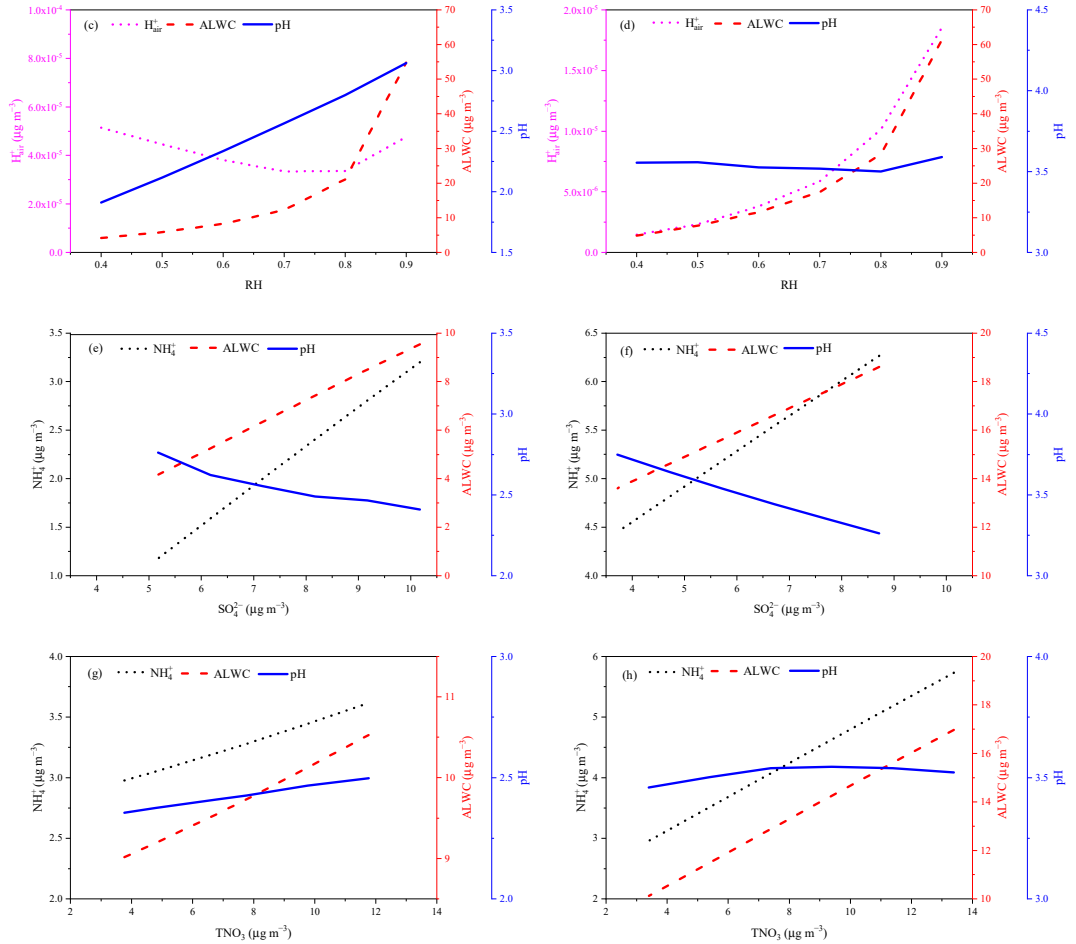

Figure 7. Sensitivity test of pH dependence on T (**a**,**b**), RH (**c**,**d**), SO4 (**e**,**f**), and TNO_3 (**g**,**h**) during summer and winter. The summer sample: Na^+ (0.08 μg m^{-3}), SO_4^{2-} (10.17 μg m^{-3}), NH_4^+ (13.32 μg m^{-3}), NO_3^- (6.77 μg m^{-3}), Cl^- (1.59 μg m^{-3}), Ca^{2+} (0.81μg m^{-3}), K^+ (0.31μg m^{-3}), Mg^{2+} (0.09 μg m^{-3}), RH (0.64), T (303.2 K). The winter sample: Na^+ (0.3 μg m^{-3}), SO_4^{2-} (5.72 μg m^{-3}), NH_4^+ (9.89 μg m^{-3}), NO_3^- (11.39 μg m^{-3}), Cl^- (1.19 μg m^{-3}), Ca^{2+} (0.14 μg m^{-3}), K^+ (0.22 μg m^{-3}), Mg^{2+} (0.05 μg m^{-3}), RH (0.65), T (284.7 K).

4. Conclusions

This study investigated the long-term trends in $PM_{2.5}$ pH in response to emission control in Shanghai. The annual average ratio of NO_3^-/SO_4^{2-} increased from 0.68 in 2010 to 1.49 in 2020, attributable to the significant reduction in SO_2 emissions and the less effective control of NOx emissions. $PM_{2.5}$ acidity showed a slightly increasing trend since the reduction in acidic emissions was partly offset by the decrease in alkaline nonvolatile cations. The monthly variation in pH values exhibited a V-shape trend, decreasing from February and increasing from September, mainly attributed to aerosol compositions and temperature which controls the partitioning of HNO_3/NH_4NO_3. The diurnal pH pattern showed a V-shaped trend with stronger fluctuation in summer than in winter due to diurnal variations in ALWC and NO_3^-/SO_4^{2-}. Atmospheric NH_3 plays a decisive role in buffering particle acidity, providing a plausible explanation on moderately acidic aerosols in the Yangtze River Delta, highly polluted with NOx emissions. Ca^{2+} and K^+ were important buffers of particle acidity and the reduction in Ca^{2+} and K^+ was responsible for the pH decline during 2010–2016.

The diurnal pH variations in summer were mainly affected by temperature and RH. The diurnal RH variations were mainly driven by temperature, underlying the decisive role of temperature in the diurnal variations in aerosol pH. In contrast, the dominant drivers of

diurnal pH variation in winter were attributed to temperature and SO_4^{2-}. Sensitivity tests showed that aerosol pH almost linearly decreased with the increase in temperature since the concentration of H^+_{air} almost exponentially increased with the increase in temperature. pH increased with the increasing RH in summer while it was not sensitive to RH in winter due to proportional increases in H^+_{air} and ALWC. pH was not very sensitive to TNO_3 in winter, indicating that reducing NOx emissions in Shanghai will not significantly affect $PM_{2.5}$ acidity in winter.

Supplementary Materials: The following supporting information can be downloaded at: https://www.mdpi.com/article/10.3390/atmos15081004/s1, Figure S1: Geographical location of the sampling sites; Figure S2: Annual variation of SO_2 and NOx emissions; Table S1: Aerosol pH of 2010–2020 with input of seasonal mean values; Table S2: Aerosol pH of 2010–2020 with input of seasonal mean values except for Ca^{2+}; Table S3: Aerosol pH of 2010–2020 with input of seasonal mean values except for K^+; Table S4: Effects of various driving factors on diurnal pH variations in the summer of 2010; Table S5. Effects of various driving factors on diurnal pH variations in the winter of 2010; Table S6. Effects of various driving factors on diurnal pH variations in the summer of 2020; Table S7. Effects of various driving factors on diurnal pH variations in the winter of 2020; Table S8. Effect of elevated TNO_3 on aerosol pH in different seasons.

Author Contributions: Validation, W.H.; investigation, Y.Y.; resources, Y.D.; writing—original draft preparation, Z.L.; writing—review and editing, X.Y. All authors have read and agreed to the published version of the manuscript.

Funding: This research was funded by the National Natural Science Foundation of China (Nos. 22176039, 21976033, and 22336001).

Institutional Review Board Statement: Not applicable.

Informed Consent Statement: Not applicable.

Data Availability Statement: The data presented in this study are available on request from the corresponding author.

Conflicts of Interest: The authors declare no conflict of interest.

References

1. Karydis, V.A.; Tsimpidi, A.P.; Pozzer, A.; Lelieveld, J. How alkaline compounds control atmospheric aerosol particle acidity. *Atmos. Chem. Phys.* **2021**, *21*, 14983–15001. [CrossRef]
2. Wang, W.; Liu, M.; Wang, T.; Song, Y.; Zhou, L.; Cao, J.; Hu, J.; Tang, G.; Chen, Z.; Li, Z.; et al. Sulfate formation is dominated by manganese-catalyzed oxidation of SO_2 on aerosol surfaces during haze events. *Nat. Commun.* **2021**, *12*, 1993. [CrossRef]
3. Zhang, S.; Li, D.; Ge, S.; Wu, C.; Xu, X.; Liu, X.; Li, R.; Zhang, F.; Wang, G. Elucidating the Mechanism on the Transition-Metal Ion-Synergetic-Catalyzed Oxidation of SO2 with Implications for Sulfate Formation in Beijing Haze. *Environ. Sci. Technol.* **2024**, *58*, 2912–2921. [CrossRef]
4. Seinfeld, J.H.; Pandis, S.N. *Atmospheric Chemistry and Physics: From Air Pollution to Climate Change*; John Wiley & Sons: Hoboken, NJ, USA, 2016.
5. Meskhidze, N. Iron mobilization in mineral dust: Can anthropogenic SO_2 emissions affect ocean productivity? *Geophys. Res. Lett.* **2003**, *30*, 2085. [CrossRef]
6. Oakes, M.; Ingall, E.D.; Lai, B.; Shafer, M.M.; Hays, M.D.; Liu, Z.G.; Russell, A.G.; Weber, R.J. Iron solubility related to particle sulfur content in source emission and ambient fine particles. *Environ. Sci. Technol.* **2012**, *46*, 6637–6644. [CrossRef] [PubMed]
7. Fang, T.; Guo, H.; Zeng, L.; Verma, V.; Nenes, A.; Weber, R.J. Highly Acidic Ambient Particles, Soluble Metals, and Oxidative Potential: A Link between Sulfate and Aerosol Toxicity. *Environ. Sci. Technol.* **2017**, *51*, 2611–2620. [CrossRef]
8. Song, X.; Wu, D.; Chen, X.; Ma, Z.; Li, Q.; Chen, J. Toxic Potencies of Particulate Matter from Typical Industrial Plants Mediated with Acidity via Metal Dissolution. *Environ. Sci. Technol.* **2024**, *58*, 6736–6743. [CrossRef]
9. Jang, M.; Czoschke, N.M.; Lee, S.; Kamens, R.M. Heterogeneous atmospheric aerosol production by acid-catalyzed particle-phase reactions. *Science* **2002**, *298*, 814–817. [CrossRef] [PubMed]
10. Cheng, Y.; Zheng, G.; Wei, C.; Mu, Q.; Zheng, B.; Wang, Z.; Gao, M.; Zhang, Q.; He, K.; Carmichael, G.; et al. Reactive nitrogen chemistry in aerosol water as a source of sulfate during haze events in China. *Sci. Adv.* **2016**, *2*, e1601530. [CrossRef] [PubMed]
11. Guo, H.; Liu, J.; Froyd, K.D.; Roberts, J.M.; Veres, P.R.; Hayes, P.L.; Jimenez, J.L.; Nenes, A.; Weber, R.J. Fine particle pH and gas–particle phase partitioning of inorganic species in Pasadena, California, during the 2010 CalNex campaign. *Atmos. Chem. Phys.* **2017**, *17*, 5703–5719. [CrossRef]

12. Yao, Y.; Ye, X.; Chen, Y.; Zhou, Y.; Lv, Z.; Wang, R.; Zheng, H.; Chen, J. Gas-particle partitioning of low-molecular-weight organic acids in suburban Shanghai: Insight into measured Henry's law constants dependent on relative humidity. *Sci. Total Environ.* **2024**, *939*, 173636. [CrossRef]
13. Ding, A.J.; Huang, X.; Nie, W.; Chi, X.G.; Xu, Z.; Zheng, L.F.; Xu, Z.N.; Xie, Y.N.; Qi, X.M.; Shen, Y.C.; et al. Significant reduction of PM2.5 in eastern China due to regional-scale emission control: Evidence from SORPES in 2011–2018. *Atmos. Chem. Phys.* **2019**, *19*, 11791–11801. [CrossRef]
14. Wang, Y.H.; Gao, W.K.; Wang, S.; Song, T.; Gong, Z.Y.; Ji, D.S.; Wang, L.L.; Liu, Z.R.; Tang, G.Q.; Huo, Y.F.; et al. Contrasting trends of PM2.5 and surface-ozone concentrations in China from 2013 to 2017. *Natl. Sci. Rev.* **2020**, *7*, 1331–1339. [CrossRef] [PubMed]
15. Wang, J.; Gao, J.; Che, F.; Wang, Y.; Lin, P.; Zhang, Y. Decade-long trends in chemical component properties of PM2.5 in Beijing, China (2011−2020). *Sci. Total Environ.* **2022**, *832*, 154664. [CrossRef]
16. Liu, M.; Song, Y.; Zhou, T.; Xu, Z.; Yan, C.; Zheng, M.; Wu, Z.; Hu, M.; Wu, Y.; Zhu, T. Fine particle pH during severe haze episodes in northern China. *Geophys. Res. Lett.* **2017**, *44*, 5213–5221. [CrossRef]
17. Tao, Y.; Murphy, J.G. The sensitivity of $PM_{2.5}$ acidity to meteorological parameters and chemical composition changes: 10-year records from six Canadian monitoring sites. *Atmos. Chem. Phys.* **2019**, *19*, 9309–9320. [CrossRef]
18. Shi, G.; Xu, J.; Peng, X.; Xiao, Z.; Chen, K.; Tian, Y.; Guan, X.; Feng, Y.; Yu, H.; Nenes, A.; et al. pH of Aerosols in a Polluted Atmosphere: Source Contributions to Highly Acidic Aerosol. *Environ. Sci. Technol.* **2017**, *51*, 4289–4296. [CrossRef]
19. Sharma, B.; Jia, S.G.; Polana, A.J.; Ahmed, M.S.; Haque, R.R.; Singh, S.; Mao, J.Y.; Sarkar, S. Seasonal variations in aerosol acidity and its driving factors in the eastern Indo-Gangetic Plain: A quantitative analysis. *Chemosphere* **2022**, *305*, 135490. [CrossRef]
20. Fu, Z.H.; Cheng, L.B.; Ye, X.N.; Ma, Z.; Wang, R.Y.; Duan, Y.; Juntao, H.; Chen, J.M. Characteristics of aerosol chemistry and acidity in Shanghai after $PM_{2.5}$ satisfied national guideline: Insight into future emission control. *Sci. Total Environ.* **2022**, *827*, 154319. [CrossRef]
21. Xie, Y.; Wang, G.; Wang, X.; Chen, J.; Chen, Y.; Tang, G.; Wang, L.; Ge, S.; Xue, G.; Wang, Y.; et al. Nitrate-dominated PM2.5 and elevation of particle pH observed in urban Beijing during the winter of 2017. *Atmos. Chem. Phys.* **2020**, *20*, 5019–5033. [CrossRef]
22. Ding, J.; Zhao, P.; Su, J.; Dong, Q.; Du, X.; Zhang, Y. Aerosol pH and its driving factors in Beijing. *Atmos. Chem. Phys.* **2019**, *19*, 7939–7954. [CrossRef]
23. Fu, X.; Guo, H.; Wang, X.; Ding, X.; He, Q.; Liu, T.; Zhang, Z. $PM_{2.5}$ acidity at a background site in the Pearl River Delta region in fall-winter of 2007–2012. *J. Hazard. Mater.* **2015**, *286*, 484–492. [CrossRef]
24. Song, S.J.; Nenes, A.; Gao, M.; Zhang, Y.Z.; Liu, P.F.; Shao, J.Y.; Ye, D.C.; Xu, W.Q.; Lei, L.; Sun, Y.L.; et al. Thermodynamic modeling suggests declines in water uptake and acidity of inorganic aerosols in Beijing winter haze events during 2014/2015–2018/2019. *Environ. Sci. Technol. Lett.* **2019**, *6*, 752–760. [CrossRef]
25. Zhou, M.; Zheng, G.; Wang, H.; Qiao, L.; Zhu, S.; Huang, D.; An, J.; Lou, S.; Tao, S.; Wang, Q.; et al. Long-term trends and drivers of aerosol pH in eastern China. *Atmos. Chem. Phys.* **2022**, *22*, 13833–13844. [CrossRef]
26. Zhang, C.; Zou, Z.; Chang, Y.; Zhang, Y.; Wang, X.; Yang, X. Source assessment of atmospheric fine particulate matter in a Chinese megacity: Insights from long-term, high-time resolution chemical composition measurements from Shanghai flagship monitoring supersite. *Chemosphere* **2020**, *251*, 126598. [CrossRef]
27. Tao, Y.; Ye, X.; Jiang, S.; Yang, X.; Chen, J.; Xie, Y.; Wang, R. Effects of amines on particle growth observed in new particle formation events. *J. Geophys. Res. Atmos.* **2016**, *121*, 324–335. [CrossRef]
28. Fountoukis, C.; Nenes, A. ISORROPIA II: A computationally efficient thermodynamic equilibrium model for K^+-Ca^{2+}-Mg^{2+}-NH_4^+-Na^+-SO_4^{2-}-NO_3^--Cl^--H_2O aerosols. *Atmos. Chem. Phys.* **2007**, *7*, 4639–4659. [CrossRef]
29. Hennigan, C.J.; Izumi, J.; Sullivan, A.P.; Weber, R.J.; Nenes, A. A critical evaluation of proxy methods used to estimate the acidity of atmospheric particles. *Atmos. Chem. Phys.* **2015**, *15*, 2775–2790. [CrossRef]
30. Song, S.; Gao, M.; Xu, W.; Shao, J.; Shi, G.; Wang, S.; Wang, Y.; Sun, Y.; McElroy, M.B. Fine-particle pH for Beijing winter haze as inferred from different thermodynamic equilibrium models. *Atmos. Chem. Phys.* **2018**, *18*, 7423–7438. [CrossRef]
31. Malm, W.C.; Day, D.E. Estimates of aerosol species scattering characteristics as a function of relative humidity. *Atmos. Environ.* **2001**, *35*, 2845–2860. [CrossRef]
32. Ye, S.; Duan, Y.; Li, Q. The trend of acidity and ion compositions of precipitation during 2000–2019 in Shanghai. *Environ. Chem.* **2021**, *40*, 3672–3680. [CrossRef]
33. Wang, G.; Zhang, R.; Gomez, M.E.; Yang, L.; Levy Zamora, M.; Hu, M.; Lin, Y.; Peng, J.; Guo, S.; Meng, J.; et al. Persistent sulfate formation from London Fog to Chinese haze. *Proc. Natl. Acad. Sci. USA* **2016**, *113*, 13630–13635. [CrossRef]
34. Guo, H.; Sullivan, A.P.; Campuzano-Jost, P.; Schroder, J.C.; Lopez-Hilfiker, F.D.; Dibb, J.E.; Jimenez, J.L.; Thornton, J.A.; Brown, S.S.; Nenes, A.; et al. Fine particle pH and the partitioning of nitric acid during winter in the northeastern United States. *J. Geophys. Res. Atmos.* **2016**, *121*, 10,355–10,376. [CrossRef]
35. Tao, M.M.; Xu, Y.; Gong, J.X.; Liu, Q.Y. Estimation of aerosol acidity at a suburban site of Nanjing using machine learning method. *J. Atmos. Chem.* **2022**, *79*, 141–151. [CrossRef]
36. Zheng, M.M.; Xu, K.; Yuan, L.X.; Chen, N.; Cao, M.H. Fine particle pH and its impact on $PM_{2.5}$ control in a megacity of central China. *Aerosol Air Qual. Res.* **2022**, *22*, 210394. [CrossRef]
37. Jia, S.G.; Chen, W.H.; Zhang, Q.; Krishnan, P.; Mao, J.Y.; Zhong, B.Q.; Huang, M.J.; Fan, Q.; Zhang, J.P.; Chang, M.; et al. A quantitative analysis of the driving factors affecting seasonal variation of aerosol pH in Guangzhou, China. *Sci. Total Environ.* **2020**, *725*, 138228. [CrossRef]

38. Guo, H.; Xu, L.; Bougiatioti, A.; Cerully, K.M.; Capps, S.L.; Hite, J.R.; Carlton, A.G.; Lee, S.H.; Bergin, M.H.; Ng, N.L.; et al. Fine-particle water and pH in the southeastern United States. *Atmos. Chem. Phys.* **2015**, *15*, 5211–5228. [CrossRef]
39. Bougiatioti, A.; Nikolaou, P.; Stavroulas, I.; Kouvarakis, G.; Weber, R.; Nenes, A.; Kanakidou, M.; Mihalopoulos, N. Particle water and pH in the eastern Mediterranean: Source variability and implications for nutrient availability. *Atmos. Chem. Phys.* **2016**, *16*, 4579–4591. [CrossRef]
40. Murphy, J.G.; Gregoire, P.K.; Tevlin, A.G.; Wentworth, G.R.; Ellis, R.A.; Markovic, M.Z.; VandenBoer, T.C. Observational constraints on particle acidity using measurements and modelling of particles and gases. *Faraday Discuss.* **2017**, *200*, 379–395. [CrossRef]
41. Guo, H.Y.; Otjes, R.; Schlag, P.; Kiendler-Scharr, A.; Nenes, A.; Weber, R.J. Effectiveness of ammonia reduction on control of fine particle nitrate. *Atmos. Chem. Phys.* **2018**, *18*, 12241–12256. [CrossRef]
42. Paglione, M.; Decesari, S.; Rinaldi, M.; Tarozzi, L.; Manarini, F.; Gilardoni, S.; Facchini, M.C.; Fuzzi, S.; Bacco, D.; Trentini, A.; et al. Historical Changes in Seasonal Aerosol Acidity in the Po Valley (Italy) as Inferred from Fog Water and Aerosol Measurements. *Environ. Sci. Technol.* **2021**, *55*, 7307–7315. [CrossRef]
43. Masiol, M.; Squizzato, S.; Formenton, G.; Khan, M.B.; Hopke, P.K.; Nenes, A.; Pandis, S.N.; Tositti, L.; Benetello, F.; Visin, F.; et al. Hybrid multiple-site mass closure and source apportionment of $PM_{2.5}$ and aerosol acidity at major cities in the Po Valley. *Sci. Total Environ.* **2020**, *704*, 135287. [CrossRef]
44. Chan, C.K.; Yao, X. Air pollution in mega cities in China. *Atmos. Environ.* **2008**, *42*, 1–42. [CrossRef]